Journal of Sound and Vibration (1996) **190**(2), 177–194

EFFECT OF MEMBER INITIAL CURVATURE ON A FLEXIBLE MECHANISM RESPONSE

K. M. Hsiao and R. T. Yang

Department of Mechanical Engineering, National Chiao Tung University, Hsinchu, Taiwan, Republic of China

(*Received* 16 *February* 1994, *and in final form* 15 *February* 1995)

A co-rotational finite element formulation of slender curved beam element is presented to investigate the effect of member initial curvature on the dynamic behaviour of planar flexible mechanisms. The Euler–Bernoulli hypothesis and the initial curvature are properly considered for the kinematics of curved beam. The nodal co-ordinates, incremental displacements and rotations, velocities, accelerations and the equations of motion of the system are defined in terms of a fixed global co-ordinate system, while the total strains in the beam element are measured in element co-ordinates which are constructed at the current configuration of the beam element. The element equations are constructed first in the element co-ordinate system and then transformed to the global co-ordinate system by using standard procedures. Both the deformation nodal forces and the inertia nodal forces of the beam element are systematically derived by consistent linearization of the non-linear beam theory in the element co-ordinates. An incremental-iterative method based on the Newmark direct integration method and the Newton–Raphson method is employed here for the solution of the non-linear dynamic equilibrium equations. Numerical examples are presented to demonstrate the effectiveness of the proposed element and to investigate the effect of the initial curvature on the dynamic response of the flexible mechanisms.

1. INTRODUCTION

The dynamic behaviour of flexible mechanisms has been the subject of considerable research [1–13]. Currently, the most popular approach for this analysis is to develop finite element models. Hsiao and Jang [13] proposed a co-rotational formulation for the dynamic analysis of planar flexible mechanisms, which was proven to be very effective by numerous numerical examples studied. However, only a straight beam element was considered.

In order to investigate the effects of member initial curvature on the dynamic behaviour of planar flexible mechanisms, a consistent co-rotational formulation of a slender curved beam with large rigid body motion and small elastic deformations is proposed in what follows here. It is assumed that the product of the initial curvature and the depth of the slender curved beam is much smaller than unity. As was done by Hsiao and Jang [10, 12], the nodal co-ordinates, incremental displacements and rotations, velocities, accelerations and the equations of motion of the system are defined in terms of a fixed global co-ordinate system, while the total strains in the beam element are measured in element co-ordinates which are constructed at the current configuration of the beam element. The element equations are constructed first in the element co-ordinate system and then transformed to the global co-ordinate system by using standard procedures. The element inertia nodal forces and deformation nodal forces are derived by using the d'Alembert principle and the virtual work principle. In order to capture all inertia effects and coupling between

0022–460X/96/070177+18 $12.00/0

extensional and flexural deformations for the curved beam element, the exact kinematics of the curved Euler beam is used in the derivation of the element inertia and deformation nodal forces. The exact expressions for the element inertia and deformation nodal forces are highly non-linear functions of the element nodal parameters. However, the dominant factors in the geometrical non-linearities of beam structures are attributable to finite rotations, the strains remaining small. For a beam structure discretized by finite elements, this implies that the motion of the individual elements to a large extent will consist of rigid body motion. If the rigid body motion part is eliminated from the total displacements and the element size is properly chosen, the deformational part (initial deformation included) of the motion is always small relative to the local element axes; thus, in conjunction with the co-rotational formulation, the higher order terms of the nodal parameters in the element deformation nodal forces and inertia nodal forces may be neglected by consistent linearization [13].

An incremental-iterative method based on the Newmark direct integration method and the Newton–Raphson method is employed here for the solution of the non-linear dynamic equilibrium equations. Numerical examples are presented to demonstrate the effectiveness of the proposed beam element and to investigate the effect of the initial curvature on the dynamic response of the flexible mechanisms.

2. NON-LINEAR FORMULATION

2.1. BASIC ASSUMPTIONS

The following assumptions are made in the derivation of the non-linear behaviour: (1) the Euler–Bernoulli hypothesis is valid; (2) the unit extension of the centroid axis of the beam element is uniform; (3) the deflections of the beam element measured in the element co-ordinates are small; (4) the product of the initial curvature and the depth of the beam is much smaller than unity; (5) the strain of the beam element is small.

The third assumption can always be satisfied if the element size is properly chosen. Due to the assumption of small strain, the engineering strain and stress are used for the measure of the strain and stress. For convenience, the engineering strain is obtained from the corresponding Green strain in this study.

2.2. CO-ORDINATE SYSTEMS

In order to describe the system, following Hsiao and Jang [10, 12], we define two sets of co-ordinate systems (see Figure 1).

(1) The first is a fixed global set of co-ordinates, X_1, X_2; the nodal co-ordinates, incremental displacements and rotations, velocities, accelerations and the equations of motion of the system are defined in this co-ordinate system.

(2) The second set is the element co-ordinates, x_1, x_2; a set of element co-ordinates associated with each element, which is constructed at the current configuration of the beam element. The origin of this co-ordinate system is located at node 1, and the x_1 axis is chosen to pass through the two end nodes of the element. *Note that this co-ordinate system is a local co-ordinate system not a moving co-ordinate system. However, this co-ordinate system is updated at each iteration*. The element equations are constructed first in the element co-ordinate system and then transformed to the global co-ordinate system for assemblage using standard procedure.

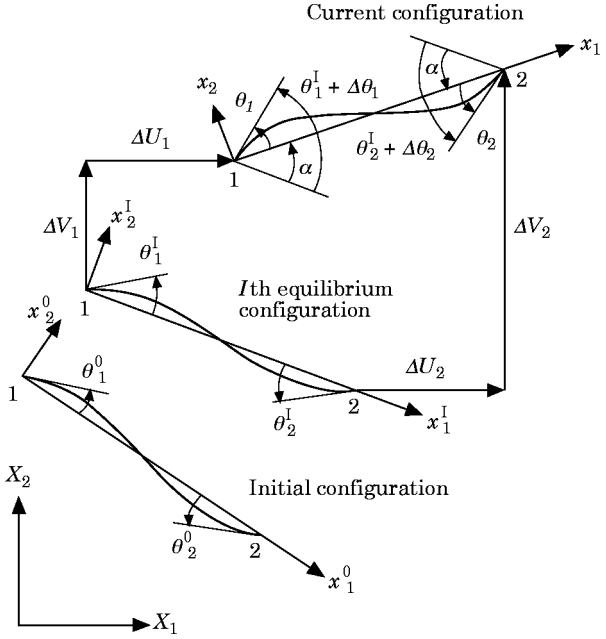

Figure 1. Co-ordinate systems.

2.3. KINEMATICS OF BEAM ELEMENTS

The geometry of the beam element is described in the current element co-ordinate system. In this study, the symbol $\{\}$ denotes a column matrix, and the symbol $(\bar{})$ denotes the variable $()$ in the undeformed state. Let P (see Figure 2) be an arbitrary point in the beam element, and Q be the point corresponding to P on the centroid axis. The position vector of point P in the undeformed and deformed configurations can be expressed as

$$\bar{\mathbf{r}} = \begin{Bmatrix} \bar{x}_p \\ \bar{y}_p \end{Bmatrix} = \begin{Bmatrix} \bar{x}_c(\bar{s}) - y \sin\bar{\theta} \\ \bar{v}(\bar{s}) + y \cos\bar{\theta} \end{Bmatrix}, \tag{1}$$

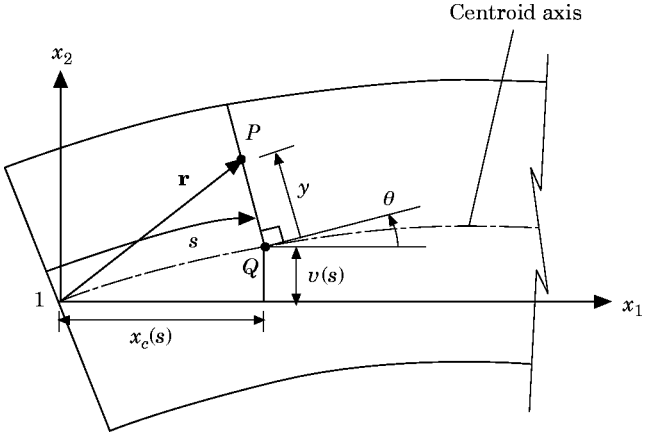

Figure 2. Kinematics of the deformed beam.

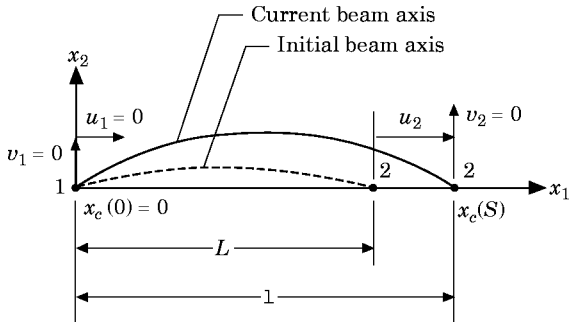

Figure 3. Nodal displacements u_1 and u_2.

and

$$\mathbf{r} = \begin{Bmatrix} x_p \\ y_p \end{Bmatrix} = \begin{Bmatrix} x_c(s) - y \sin\theta \\ v(s) + y \cos\theta \end{Bmatrix}, \tag{2}$$

where $x_c(s)$ and $v(s)$ are the x_1 and x_2 co-ordinates of point Q, respectively, s is the arc length of the deformed centroid axis measured from node 1 to point Q, y is the distance between points P and Q, and θ is the angle measured from the x_1-axis to the tangent of the centroid axis. The relationship among $x_c(s)$ and $v(s)$ and s may be given as

$$x_c(s) = u_1 + \frac{S}{2}\int_{-1}^{\xi} \cos\theta \, \mathrm{d}\xi, \qquad \cos\theta = (1 - v'^2)^{1/2}, \qquad v' = \frac{\mathrm{d}v(s)}{\mathrm{d}s} = \sin\theta,$$

$$\xi = 1 + \frac{2s}{S}, \tag{3–6}$$

where u_1 is the displacement of node 1 in the x_1-direction, S is the current arc length of the centroid axis of the beam element. Note that due to the definition of the element co-ordinate system, the value of u_1 is equal to zero. However, the variation and time derivatives of u_1 are not zero. Making use of equation (3), one obtains

$$S = 2l \Big/ \int_{-1}^{1} \cos\theta \, \mathrm{d}\xi = 2l/\beta \qquad \text{and} \qquad l = x_c(S) - x_c(0) = L - u_1 + u_2, \tag{7, 8}$$

in which l is the current chord length of the beam axis, L is the chord length of the undeformed beam axis, and u_2 is the displacement of node 2 in the x_1-direction as shown in Figure 3.

If $\bar{s}$ and y in equation (1) are regarded as the Lagrange co-ordinates, the Green strains ϵ_{ij} $(i = 1, 2; j = 1, 2)$ are given by [14]

$$\epsilon_{ij} = \tfrac{1}{2}(\mathbf{G}_i^{\mathrm{T}}\mathbf{G}_j - \mathbf{g}_i^{\mathrm{T}}\mathbf{g}_j), \tag{9}$$

where

$$\mathbf{G}_1 = \frac{\partial \mathbf{r}}{\partial \bar{s}} = \frac{\partial \mathbf{r}}{\partial s}\frac{\partial s}{\partial \bar{s}} = (1 + \epsilon_0)(1 - \kappa y)\begin{Bmatrix} \cos\theta \\ \sin\theta \end{Bmatrix}, \qquad \mathbf{G}_2 = \frac{\partial \mathbf{r}}{\partial y} = \begin{Bmatrix} -\sin\theta \\ \cos\theta \end{Bmatrix},$$
$$\mathbf{g}_1 = \frac{\partial \bar{\mathbf{r}}}{\partial \bar{s}} = (1 - \bar{\kappa} y)\begin{Bmatrix} \cos\bar{\theta} \\ \sin\bar{\theta} \end{Bmatrix}, \qquad \mathbf{g}_2 = \frac{\partial \bar{\mathbf{r}}}{\partial y} = \begin{Bmatrix} -\sin\bar{\theta} \\ \cos\bar{\theta} \end{Bmatrix}, \tag{10}$$

$$\epsilon_0 = (\partial s/\partial \bar{s}) - 1 \qquad \text{and} \qquad \kappa = \partial\theta/\partial s = v''/\cos\theta = cv'', \tag{11, 12}$$

in which ϵ_0 is the unit extension of the centroid axis, $c = 1/\cos\theta$, $v'' = \mathrm{d}^2v/\mathrm{d}s^2$, and κ is an exact expression for the physical curvature of the deformed beam centroid axis. An equivalent expression for κ has been given by Hodges [15]. Making use of the assumption of uniform unit extension, one may rewrite the unit extension ϵ_0 in equation (11) as

$$\epsilon_0 = (S/\bar{S}) - 1. \tag{13}$$

Due to the use of the Euler–Bernoulli hypothesis, as expected, ϵ_{11} is the only non-zero component of ϵ_{ij}, and is given by

$$\epsilon_{11} = \tfrac{1}{2}[(1+\epsilon_0)^2(1-\kappa y)^2 - (1-\bar{\kappa} y)^2]. \tag{14}$$

The engineering strain corresponding to ϵ_{11} is given by [14]

$$\epsilon = \left(1 + \frac{2\epsilon_{11}}{\mathbf{g}_1^{\mathrm{T}}\mathbf{g}_1}\right)^{1/2} - 1 = \frac{(1+\epsilon_0)(1-\kappa y)}{(1-\bar{\kappa} y)} - 1. \tag{15}$$

Note that ϵ in equation (15) is an exact expression for the engineering strain for the curved Euler beam. When $\bar{\kappa} y \ll 1$, the engineering strain in equation (15) may be approximated by $\epsilon \approx \epsilon_0 - (\kappa - \bar{\kappa}) y$.

Here, the lateral deflection of the centroid axis, $v(s)$ is assumed to be represented by cubic Hermitian polynomials in s and is given by

$$v(s) = \{N_1, N_2, N_3, N_4\}^{\mathrm{T}}\{v_1, v_1', v_2, v_2'\} = \mathbf{N}_{\mathrm{b}}^{\mathrm{T}}\mathbf{u}_{\mathrm{b}}, \tag{16}$$

where v_j and v_j' ($j = 1, 2$) are the nodal values of v and v' at nodes, j, respectively. Note that, due to the definition of the element co-ordinates, the value of v_j is zero. However, the variations and time derivatives of v_j are not zero. N_i ($i = 1$–4) are shape functions and are given by

$$N_1 = \tfrac{1}{4}(1-\xi)^2(2+\xi), \qquad N_2 = (S/8)(1-\xi^2)(1-\xi), \qquad N_3 = \tfrac{1}{4}(1+\xi)^2(2-\xi),$$
$$N_4 = (S/8)(-1+\xi^2)(1+\xi), \tag{17}$$

where S is the current arc length of the centroid axis, and ξ is the non-dimensional co-ordinate defined in equation (6).

The initial lateral deflection of the centroid axis, $\bar{v}(\bar{s})$ is required for the calculation of the initial curvature $\bar{\kappa}$ of the beam axis. For consistency, $\bar{v}(\bar{s})$, should have the same form as $v(s)$. Here $\bar{v}(\bar{s})$ is obtained by adding an overbar for each variable in equations (6), (16) and (17).

Note that because the value of v_j is zero, from equations (16) and (17), v' in equation (5) can be determined by v_j' and ξ only. Thus, the value of S in equation (7) can be calculated by using equations (7), (8), (16) and (17), and then $x_c(s)$ in equation (3) can be determined by using v' and S.

2.4. NODAL PARAMETERS AND NODAL FORCES

The global nodal parameters for the system of equations associated with the individual elements are chosen to be the incremental translations ΔU_j and ΔV_j ($j = 1, 2$) in the X_1 and X_2 directions, respectively, and the incremental counterclockwise rotations $\Delta\theta_j$ ($j = 1, 2$) at nodes j (see Figures 1 and 4). The nodal forces corresponding to the nodal parameters ΔU_j, ΔV_j and $\Delta\theta_j$ ($j = 1, 2$) at nodes j are forces F_{ij} in X_i ($i = 1, 2$) directions and counterclockwise moments m_j ($j = 1, 2$) at nodes j (see Figure 4). The element employed here has three degrees of freedom per node defined in the current element co-ordinate system (see Figures 1, 3 and 4): these are the translations u_j and v_j ($j = 1, 2$)

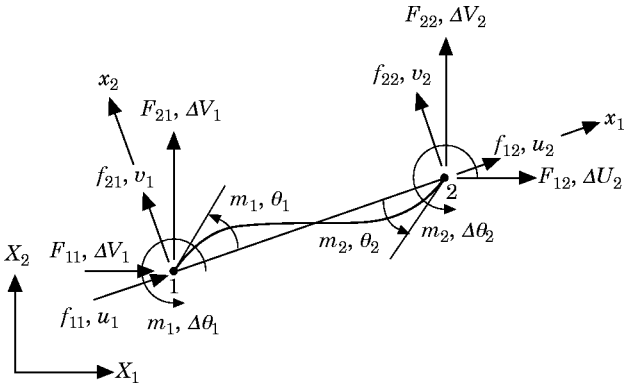

Figure 4. Nodal parameters and nodal forces.

in the x_1 and x_2 directions, respectively, and the counterclockwise rotations θ_j ($j=1, 2$) at nodes j. Note that the initial rotations are included in the measurement of θ_j. The nodal forces corresponding to the nodal parameters u_j and v_j and θ_j ($j=1, 2$) at nodes j are forces f_{ij} in x_i ($i=1, 2$) directions and counterclockwise moments m_j ($j=1, 2$) at nodes j (see Figure 4).

Due to the definition of the element co-ordinate system, the non-zero element nodal parameters are u_2 and θ_j ($j=1, 2$) only. Let θ_j^I, X_{1j}^I and X_{2j}^I ($j=1, 2$), and x_i^I ($i=1, 2$) be the total nodal rotations, global nodal co-ordinates in the X_1 and X_2 axes at nodes j, and the axes of the element co-ordinate system, respectively, for a single element at the equilibrium configuration of the Ith increment. The procedure used to determine the current u_2 and θ_j ($j=1, 2$) for individual elements corresponding to the incremental translations ΔU_j and ΔV_j ($j=1, 2$), and the incremental nodal rotations $\Delta\theta_j$ ($j=1, 2$) at nodes j (see Figure 1) is the same as that given in reference [12]. However, it is repeated here for completeness.

X_{1j} and X_{2j} ($j=1, 2$), the current global nodal co-ordinates of the element at nodes j, are obtained by adding ΔU_j and ΔV_j to X_{1j}^I and X_{2j}^I, respectively, and then the x_i ($i=1, 2$) axes, the axes of the current element co-ordinate system, can be constructed. The current chord length of the element l can be calculated by $l=[(X_{12}-X_{11})^2+(X_{22}-X_{21})^2]^{1/2}$, and then the value of u_2 can be determined by $u_2=l-L$, where L is the initial chord length of the element. Let α (Figure 1) denote the angle of rigid body rotation measured from the x_1^I-axis to the current x_1-axis; then the current value of θ_j ($j=1, 2$) is given by $\theta_j=\theta_j^I+\Delta\theta_j-\alpha$.

2.5. ELEMENT INTERNAL NODAL FORCE VECTORS

The element internal nodal forces are obtained from the d'Alembert principle and the virtual work principle in the current element co-ordinate system. The virtual work principle requires that

$$\delta\mathbf{u}_a^T\mathbf{f}_a+\delta\mathbf{u}_b^{\theta T}\mathbf{f}_b=\int_{\bar{V}}(\delta\epsilon^T\sigma+\rho\delta\mathbf{r}^T\ddot{\mathbf{r}})\,d\bar{V}, \tag{18}$$

where

$$\delta\mathbf{u}_a=\{\delta u_1, \delta u_2\}, \qquad \delta\mathbf{u}_b^{\theta}=\{\delta v_1, \delta\theta_1, \delta v_2, \delta\theta_2\}, \tag{19}$$

$$\mathbf{f}_a=\mathbf{f}_a^d+\mathbf{f}_a^i=\{f_{11}, f_{12}\}, \qquad \mathbf{f}_b=\mathbf{f}_b^d+\mathbf{f}_b^i=\{f_{21}, m_1, f_{22}, m_2\}, \tag{20}$$

in which $\mathbf{f}_j^{\mathrm{d}}$ and $\mathbf{f}_j^{\mathrm{i}}$ (j = a, b) are the deformation nodal force vector and the inertia nodal force vector, respectively. $\delta\epsilon$ is the variation of ϵ given in equation (15). $\sigma = E\epsilon$ is the normal stress, where E is the Young's modulus. ρ is the density, $\delta\mathbf{r}$ is the variation of $\mathbf{r}$ given in equation (2) with respect to the nodal parameters, and $\ddot{\mathbf{r}} = \mathrm{d}^2\mathbf{r}/\mathrm{d}t^2$. In this paper, the symbol ($\dot{}$) denotes differentiation with respect to time t. $\bar{V}$ is the volume of the undeformed beam. For a curved beam the differential volume $\mathrm{d}\bar{V}$ may be expressed as $\mathrm{d}\bar{V} = (1-\bar{\kappa}y)\,\mathrm{d}A\,d\bar{s} = (1-\bar{\kappa}y)\,\mathrm{d}A\,\mathrm{d}s/(1+\epsilon_0)$, where $\mathrm{d}A$ is the differential cross section area.

Note that the element co-ordinate system is just a local co-ordinate system, which is updated at each iteration, not a moving co-ordinate system. Thus, $\ddot{\mathbf{r}}$ *is the absolute acceleration and* $\int_{\bar{V}} \rho\delta\mathbf{r}^{\mathrm{T}}\ddot{\mathbf{r}}\,\mathrm{d}\bar{V}$ *comprises all the virtual inertia forces.*

The exact expressions for $\mathbf{f}_{\mathrm{a}}$ and $\mathbf{f}_{\mathrm{b}}$ may be obtained by substituting the exact expressions for $\delta\epsilon$, ϵ, $\delta\mathbf{r}$ and $\ddot{\mathbf{r}}$ into equation (18). However, if the element size is properly chosen, the values of the nodal parameters (displacements and rotations) of the element defined in the current element co-ordinate system, which are the total deformational displacements and rotations, may always be much smaller than unity. Thus only the first order terms of the nodal parameters are retained in $\mathbf{f}_{\mathrm{a}}^{\mathrm{d}}$ and $\mathbf{f}_{\mathrm{b}}^{\mathrm{d}}$. However, in order to include the effect of axial force on the lateral forces, a second order term of the nodal parameters is retained in $\mathbf{f}_{\mathrm{b}}^{\mathrm{d}}$. Because the values of the nodal parameters of the element may always be much smaller than unity, it is reasonable to assume that the coupling between the nodal parameters and their time derivatives are negligible. Thus only zeroth order terms of nodal parameters are retained in $\mathbf{f}_{\mathrm{a}}^{\mathrm{i}}$ and $\mathbf{f}_{\mathrm{b}}^{\mathrm{i}}$. The approximations, $1-\bar{\kappa}y \approx 1$, $1+\epsilon_0 \approx 1$, $v' \approx \theta$, $\dot{v}' \approx \theta$, $\ddot{v}' \approx \ddot{\theta}$ and $\cos\theta \approx 1$ are used in the derivation of $\mathbf{f}_{\mathrm{a}}$ and $\mathbf{f}_{\mathrm{b}}$. In order to avoid improper omission in the derivation of $\mathbf{f}_{\mathrm{a}}$ and $\mathbf{f}_{\mathrm{b}}$, these approximations are applied to the exact expressions for $\delta\epsilon$, ϵ, $\delta\mathbf{r}$ and $\ddot{\mathbf{r}}$. Note that because the shape functions of v' and v'' are functions of S, which is given in equation (7), the variations and differentiation of the shape functions are considered here.

From equations (7), (8), (12), (13) and (15), $\delta\epsilon$ may be expressed as

$$\delta\epsilon = [1/(1-\bar{\kappa}y)][(1-\kappa y)\delta\epsilon_0 - (1+\epsilon_0)y\delta\kappa], \tag{21}$$

where

$$\delta\kappa = c\delta v'' + c^3 v' v'' \delta v', \qquad \delta\epsilon_0 = \delta S/\bar{S} = (2\delta l/\beta\bar{S}) - (2l\delta\beta/\beta^2\bar{S}), \tag{22, 23}$$

$$\delta l = \{-1,\ 1\}^{\mathrm{T}}\{\delta u_1,\ \delta u_2\} = \mathbf{G}_{\mathrm{a}}^{\mathrm{T}}\delta\mathbf{u}_{\mathrm{a}}, \qquad \delta\beta = -\int_{-1}^{1} cv'\delta v'\,\mathrm{d}\xi, \tag{24, 25}$$

in which $\delta v'$ and $\delta v''$ are the variations of v' and v'', respectively, with respect to the nodal parameters. From equations (16) and (17), $\delta v'$ and $\delta v''$ can be obtained as

$$\delta v' = (\delta\mathbf{N}_{\mathrm{b}}'^{\mathrm{T}})\mathbf{u}_{\mathrm{b}} + \mathbf{N}_{\mathrm{b}}^{\mathrm{T}}\delta\mathbf{u}_b = -[\delta\epsilon_0/(1-\epsilon_0)]\mathbf{N}_{\mathrm{c}}^{\mathrm{T}}\mathbf{u}_{\mathrm{b}} + \mathbf{N}_{\mathrm{b}}'^{\mathrm{T}}\delta\mathbf{u}_{\mathrm{b}}, \tag{26}$$

and

$$\delta v'' = (\delta\mathbf{N}_{\mathrm{b}}''^{\mathrm{T}})\mathbf{u}_{\mathrm{b}} + \mathbf{N}_{\mathrm{b}}''^{\mathrm{T}}\delta\mathbf{u}_{\mathrm{b}} = -[\delta\epsilon_0/(1+\epsilon_0)]\mathbf{N}_{\mathrm{d}}^{\mathrm{T}}\mathbf{u}_{\mathrm{b}} + \mathbf{N}_{\mathrm{b}}''^{\mathrm{T}}\delta\mathbf{u}_{\mathrm{b}}, \tag{27}$$

where

$$\delta\mathbf{u}_{\mathrm{b}} = \{\delta v_1,\ \cos\theta_1\delta\theta_1,\ \delta v_2,\ \cos\theta_2\delta\theta_2\}, \qquad \mathbf{N}_{\mathrm{c}} = \{N_1',\ 0,\ N_3',\ 0\},$$
$$\mathbf{N}_{\mathrm{d}} = \{2N_1'',\ N_2'',\ 2N_3'',\ N_4''\}. \tag{28–30}$$

Note that due to the definition of the element co-ordinate system, the values of v_1 and v_2 are zero. Thus $\mathbf{N}_{\mathrm{c}}^{\mathrm{T}}\mathbf{u}_{\mathrm{b}} = 0$ in equation (26), and $\mathbf{N}_{\mathrm{d}}^{\mathrm{T}}\mathbf{u}_{\mathrm{b}} = v''$ in equation (27).

From equations (22)–(30), by using the approximations $1-\bar{\kappa}y\approx 1$, $1+\epsilon_0\approx 1$, $v'\approx\theta$, and $\cos\theta\approx 1$, and retaining all zeroth order terms and one first-order term of the nodal parameters, $\delta\epsilon$ in equation (21) may be approximated by

$$\delta\epsilon=(1/\bar{S})\mathbf{G}_{\mathrm{a}}^{\mathrm{T}}\delta\mathbf{u}_{\mathrm{a}}+\mathbf{G}_{\mathrm{b}}^{\mathrm{T}}\delta\mathbf{u}_{\mathrm{b}}^{\theta}-y\mathbf{N}_{\mathrm{b}}''^{\mathrm{T}}\delta\mathbf{u}_{\mathrm{b}}^{\theta}, \tag{31}$$

where

$$\mathbf{G}_{\mathrm{b}}=\tfrac{1}{2}\int_{-1}^{1}v'\mathbf{N}_{\mathrm{b}}'\,\mathrm{d}\xi. \tag{32}$$

From equations (2)–(8), (16) and (17), $\delta\mathbf{r}$ can be expressed as

$$\delta\mathbf{r}=\begin{Bmatrix}\delta u_1+\dfrac{\delta S}{2}\displaystyle\int_{-1}^{\xi}(1-v'^2)^{1/2}\,\mathrm{d}\xi-\frac{S}{2}\int_{-1}^{\xi}cv'\,\delta v'\,\mathrm{d}\xi-y\delta v'\\ \delta v-ycv'\delta v'\end{Bmatrix}, \tag{33}$$

where

$$\delta v=(\delta\mathbf{N}_{\mathrm{b}}^{\mathrm{T}})\mathbf{u}_{\mathrm{b}}+\mathbf{N}_{\mathrm{b}}^{\mathrm{T}}\delta\mathbf{u}_{\mathrm{b}}=[\delta\epsilon_0/(1+\epsilon_0)]\mathbf{N}_{\mathrm{e}}^{\mathrm{T}}\mathbf{u}_{\mathrm{b}}+\mathbf{N}_{\mathrm{b}}^{\mathrm{T}}\delta\mathbf{u}_{\mathrm{b}}\qquad\text{and}\qquad\mathbf{N}_{\mathrm{e}}=\{0,\,N_2,\,0,\,N_4\}. \tag{35}$$

Substituting equations (23)–(26) and (34) into equation (33), using the approximations $1+\epsilon_0\approx 1$, $v'\approx\theta$, and $\cos\theta\approx 1$, and retaining only zeroth order terms of nodal parameters, one obtains

$$\delta\mathbf{r}=\begin{Bmatrix}\mathbf{N}_{\mathrm{a}}^{\mathrm{T}}\delta\mathbf{u}_{\mathrm{a}}-y\mathbf{N}_{\mathrm{b}}'^{\mathrm{T}}\delta\mathbf{u}_{\mathrm{b}}^{\theta}\\ \mathbf{N}_{\mathrm{b}}^{\mathrm{T}}\delta\mathbf{u}_{\mathrm{b}}^{\theta}\end{Bmatrix},\qquad\text{where}\qquad\mathbf{N}_{\mathrm{a}}=\left\{\frac{1-\xi}{2},\,\frac{1+\xi}{2}\right\}. \tag{36, 37}$$

From equations (2)–(8), (16) and (17), the exact expression for $\ddot{\mathbf{r}}$ may be obtained. Using the approximations $1+\epsilon_0\approx 1$, $v'\approx\theta$, $\dot{v}\approx\dot{\theta}$, $\ddot{v}'\approx\ddot{\theta}$ and $\cos\theta\approx 1$, and retaining only zeroth order terms of nodal parameters in the exact expression of $\ddot{\mathbf{r}}$, one obtains

$$\ddot{\mathbf{r}}=\begin{Bmatrix}\mathbf{N}_{\mathrm{a}}^{\mathrm{T}}\ddot{\mathbf{u}}_{\mathrm{a}}+\dfrac{\bar{S}(1+\xi)}{4}\displaystyle\int_{-1}^{1}(\mathbf{N}_{\mathrm{b}}'^{\mathrm{T}}\mathbf{u}_{\mathrm{b}})^2\,\mathrm{d}\xi-\frac{\bar{S}}{2}\int_{-1}^{\xi}(\mathbf{N}_{\mathrm{b}}'^{\mathrm{T}}\dot{\mathbf{u}}_{\mathrm{b}})^2\,\mathrm{d}\xi+\frac{2y}{\bar{S}}\mathbf{N}_{\mathrm{c}}^{\mathrm{T}}\dot{\mathbf{u}}_{\mathrm{b}}\mathbf{G}_{\mathrm{a}}^{\mathrm{T}}\dot{\mathbf{u}}_{\mathrm{a}}-y\mathbf{N}_{\mathrm{b}}'^{\mathrm{T}}\ddot{\mathbf{u}}_{\mathrm{b}}\\ \mathbf{N}_{\mathrm{b}}^{\mathrm{T}}\ddot{\mathbf{u}}_{\mathrm{b}}-y(\mathbf{N}_{\mathrm{b}}'^{\mathrm{T}}\dot{\mathbf{u}}_{\mathrm{b}})^2+\dfrac{2}{\bar{S}}\mathbf{G}_{\mathrm{a}}^{\mathrm{T}}\dot{\mathbf{u}}_{\mathrm{a}}\mathbf{N}_{\mathrm{e}}^{\mathrm{T}}\dot{\mathbf{u}}_{\mathrm{b}}\end{Bmatrix}, \tag{38}$$

where

$$\dot{\mathbf{u}}_{\mathrm{a}}=\{\dot{u}_1,\,\dot{u}_2\},\qquad\ddot{\mathbf{u}}_{\mathrm{a}}=\{\ddot{u}_1,\,\ddot{u}_2\},\qquad\text{and}\qquad\dot{\mathbf{u}}_{\mathrm{b}}=\{\dot{v}_1,\,\dot{\theta}_1,\,\dot{v}_2,\,\dot{\theta}_2\},$$
$$\ddot{\mathbf{u}}_{\mathrm{b}}=\{\ddot{v}_1,\,\ddot{\theta}_1,\,\ddot{v}_2,\,\ddot{\theta}_2\}. \tag{39, 40}$$

Note that $\dot{\mathbf{u}}_j$ and $\ddot{\mathbf{u}}_j$ ($j=$ a, b) are the absolute velocity and acceleration vectors of an element referred to the element co-ordinate system which are obtained from the transformation of the corresponding global velocity and acceleration vectors extracted from the equations of motion of the system by using standard procedures [9].

Substituting equations (15), (31), (36) and (38) into equation (18), using the approximations $1-\bar{\kappa}y\approx 1$, $1+\epsilon_0\approx 1$, $v'\approx\theta$, and $\cos\theta\approx 1$, dropping higher order terms

of nodal parameters, and equating the terms in both sides of equation (18) corresponding to virtual displacement vectors $\delta\mathbf{u}_a$ and $\delta\mathbf{u}_b^\theta$, respectively, one obtains

$$\mathbf{f}_a^d = AE\epsilon_0\mathbf{G}_a, \qquad \mathbf{f}_b^d = \mathbf{k}_g\mathbf{u}_b + \mathbf{k}_b(\mathbf{u}_b - \bar{\mathbf{u}}_b), \tag{41}$$

$$\mathbf{k}_b = \frac{EI\bar{S}}{2}\int_{-1}^{1}\mathbf{N}_b''\mathbf{N}_b''^{\mathrm{T}}\,\mathrm{d}\xi, \qquad \mathbf{k}_g = \frac{AE\epsilon_0\bar{S}}{2}\int_{-1}^{1}\mathbf{N}_b'\mathbf{N}_b'^{\mathrm{T}}\,\mathrm{d}\xi, \tag{42}$$

$$\mathbf{f}_a^i = \mathbf{m}_a\ddot{\mathbf{u}}_a + \underline{\frac{\rho A\bar{S}}{2}\int_{-1}^{1}\mathbf{N}_a\left[\frac{\bar{S}(1+\xi)}{4}\int_{-1}^{1}(\mathbf{N}_b'^{\mathrm{T}}\dot{\mathbf{u}}_b)^2\,\mathrm{d}\xi - \frac{\bar{S}}{2}\int_{-1}^{\xi}(\mathbf{N}_b'^{\mathrm{T}}\dot{\mathbf{u}}_b)^2\,\mathrm{d}\xi\right]\mathrm{d}\xi},$$

$$\mathbf{m}_a = \frac{\rho A\bar{S}}{2}\int_{-1}^{1}\mathbf{N}_a\mathbf{N}_a^{\mathrm{T}}\,\mathrm{d}\xi, \tag{43}$$

$$\mathbf{f}_b^i = \mathbf{m}_t\ddot{\mathbf{u}}_b + \mathbf{m}_r\ddot{\mathbf{u}}_b + \underline{\rho A\mathbf{G}_a^{\mathrm{T}}\dot{\mathbf{u}}_a\int_{-1}^{1}\mathbf{N}_b\mathbf{N}_c^{\mathrm{T}}\,\mathrm{d}\xi\;\dot{\mathbf{u}}_b - \rho I\mathbf{G}_a^{\mathrm{T}}\dot{\mathbf{u}}_a\int_{-1}^{1}\mathbf{N}_b'\mathbf{N}_c^{\mathrm{T}}\,\mathrm{d}\xi\;\dot{\mathbf{u}}_b},$$

$$\mathbf{m}_t = \frac{\rho A\bar{S}}{2}\int_{-1}^{1}\mathbf{N}_b\mathbf{N}_b^{\mathrm{T}}\,\mathrm{d}\xi, \qquad \mathbf{m}_r = \frac{\rho I\bar{S}}{2}\int_{-1}^{1}\mathbf{N}_b'\mathbf{N}_b'^{\mathrm{T}}\,\mathrm{d}\xi, \tag{44}$$

where A is the cross-section area, $I = \int_A y^2\,\mathrm{d}A$. ϵ_0 in equations (41) and (42) is given in equation (13). $\mathbf{K}_b$ and $\mathbf{k}_g$ in equation (42) are bending and geometric stiffness matrices of conventional beam element [12]. $\mathbf{m}_a$ in equations (43) is the consistent mass matrix of bar element [12]. $\mathbf{m}_t$ and $\mathbf{m}_r$ in equations (44) are the consistent mass matrices of conventional beam element for lateral translation and rotation, respectively [12]. The underlined terms in equations (43) and (44) are called velocity coupling terms in this study.

Note that even equations (42)–(44) are functions of S, because the approximation $1+\epsilon_0 \approx 1$ is used in the derivation of equations (42)–(44); S is approximated by $\bar{S}$ in equations (42)–(44).

2.6. ELEMENT MATRICES

The element stiffness matrices and mass matrices may be obtained by differentiating the element nodal force vectors in equations (41)–(44) with respect to nodal parameters, and time derivatives of nodal parameters. However, element matrices are used only to obtain predictors and correctors for incremental solutions of the non-linear equations in this study. Approximate element matrices can meet these requirements. Thus, the conventional stiffness matrix of a bar element

$$\mathbf{k}_a = \frac{AE}{\bar{S}}\begin{bmatrix} 1 & -1 \\ -1 & 1 \end{bmatrix}, \tag{45}$$

and conventional element matrices given in equations (41)–(44) are adopted here for simplicity.

2.7. EQUATIONS OF MOTION

The non-linear equations of motion may be expressed as [13]

$$\mathbf{R} = \mathbf{F}^{\mathrm{I}} + \mathbf{F}^{\mathrm{D}} - \mathbf{P} = \mathbf{0}, \tag{46}$$

where $\mathbf{R}$ is the unbalanced force among the inertia nodal force $\mathbf{F}^{\mathrm{I}}$, deformational nodal force $\mathbf{F}^{\mathrm{D}}$, and the external nodal force $\mathbf{P}$. $\mathbf{F}^{\mathrm{I}}$ and $\mathbf{F}^{\mathrm{D}}$ are assembled from the element nodal force vectors in equations (41)–(44), which must be transformed from element co-ordinate system to global co-ordinate system before assemblage by using standard procedures.

In this paper, three convergence criteria are employed for the equilibrium iterations, and these are given by

$$e_f = \|R\|/N\|R_i\| \leqslant e_{ftol}, \qquad e_d = \|\Delta U\|/N\|\Delta U_i\| \leqslant e_{dtol},$$

$$e_w = \|R^{\mathrm{T}}\Delta U\|/N\|R_{\mathrm{i}}^{\mathrm{T}}\Delta U_{\mathrm{i}}\| \leqslant e_{wtol}, \tag{47–49}$$

where the subscript i of a quantity is used to denote that the quantity corresponds to the ith iteration; N is number of the equations of the system; $\Delta\mathbf{U}$ is the displacement correction; e_{ftol}, e_{dtol} and e_{wtol} are prescribed values of error tolerance. The error tolerance is set to 10^{-10}, and i is chosen to be 1 in this paper.

3. NUMERICAL ALGORITHM

An incremental iterative method based on the Newmark direct integration method [12, 16] and the Newton–Raphson method is employed. For clearness, the numerical procedure used here is given as follows.

Assume that the dynamic equilibrium configuration at time t_n is known. Let $\dot{\mathbf{Q}}_n$ and $\ddot{\mathbf{Q}}_n$ denote the velocity and acceleration vectors of the discretized system at time t_n, respectively. $\Delta\mathbf{Q}$, $\dot{\mathbf{Q}}_{n+1}$ and $\ddot{\mathbf{Q}}_{n+1}$, the incremental displacement, velocity and acceleration vectors at time $t_{n+1} = t_n + \Delta t$, respectively, may be obtained by the following incremental-iterative procedure.

The initial incremental displacement vector $\Delta\mathbf{Q}$ for the next time step may be chosen to be $\Delta\mathbf{Q} = \mathbf{0}$. Then, from the Newmark method, $\dot{\mathbf{Q}}_{n+1}$ and $\ddot{\mathbf{Q}}_{n+1}$ can be expressed as

$$\ddot{\mathbf{Q}}_{n+1} = \frac{\Delta\mathbf{Q}}{a\Delta t^2} - \frac{\dot{\mathbf{Q}}_n}{a\Delta t} - \left(\frac{1}{2a} - 1\right)\ddot{\mathbf{Q}}_n, \qquad \text{and} \qquad \dot{\mathbf{Q}}_{n+1} = \dot{\mathbf{Q}}_n + \Delta t[(1-b)\ddot{\mathbf{Q}}_n + b\ddot{\mathbf{Q}}_{n+1}], \tag{50, 51}$$

where Δt is the time step size, and a and b are the parameters of the Newmark method. In the present study $a = 0{\cdot}25$ and $b = 0{\cdot}5$ are employed.

The incremental translations ΔU_j and ΔV_j, and the incremental nodal rotations $\Delta\theta_j$ ($j = 1, 2$) of individual elements at element nodes j can be extracted from $\Delta\mathbf{Q}$. By using the method described in section 2.4, the current configuration and deformation of individual elements can be calculated. Then, by using equations (41) and (42), the element deformation nodal force vectors can be calculated in the current element co-ordinate system.

One can extract the global velocity and acceleration vectors of individual elements at element nodes j ($j = 1, 2$) from $\dot{\mathbf{Q}}_{n+1}$ and $\ddot{\mathbf{Q}}_{n+1}$. Then, the absolute velocity and acceleration vectors (equations (39) and (40)), of individual elements, referred to the element co-ordinate system, can be obtained from the transformation of the corresponding global velocity and acceleration vectors to the current element co-ordinate system by using standard procedures. Then, by using equations (43) and (44), the element inertia nodal force vectors can be calculated in the current element co-ordinate system.

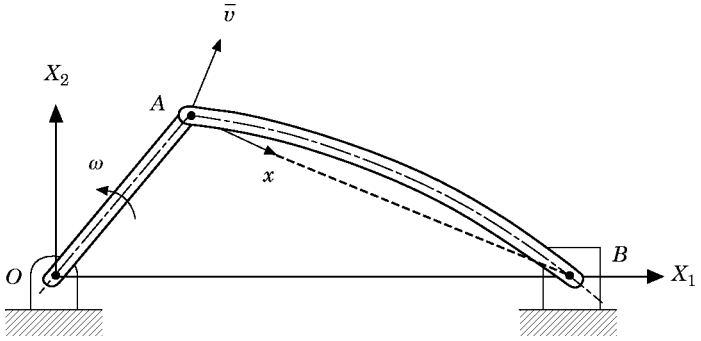

Figure 5. Slider–crank mechanism.

From the assemblage of the element nodal force vectors and equation (46), the unbalanced force vector **R** can be calculated. If the convergence criteria in equations (47)–(49) are not satisfied, a displacement correction $\Delta\mathbf{U}$ is added to the previous $\Delta\mathbf{Q}$ to obtain a new incremental displacement for the next iteration. The displacement correction $\Delta\mathbf{U}$ may be determined by using the Newton–Raphson method as

$$\Delta\mathbf{U} = -\hat{\mathbf{K}}^{-1}\mathbf{R} \tag{52}$$

where $\hat{\mathbf{K}}$ is the co-called effective stiffness matrix and may be expressed by

$$\hat{\mathbf{K}} = (1/a\Delta t^2)\mathbf{M} + \mathbf{K}, \tag{53}$$

where a is the parameter of the Newmark method. **M** and **K** are the mass matrix and the stiffness matrix of the system of equations, which are assembled from element matrices. This procedure is repeated until the convergence criteria are satisfied.

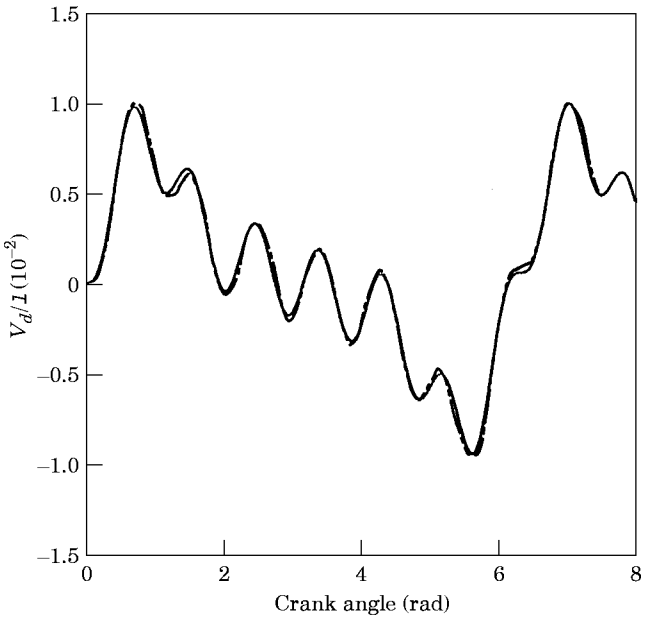

Figure 6. Midpoint deflection of coupler for slider-crank mechanism for $\omega = 124{\cdot}8$ rad/s, $\eta/l = 0$ and $m_s = 0$. ——, present; —·—, Chu and Pan [1].

4. NUMERICAL STUDIES

4.1. SLIDER–CRANK MECHANISM

A slide–crank mechanism as shown in Figure 5 consists of a rigid crank OA, an initially curved flexible coupler AB of uniform circular cross-section, and a sliding block located at B. The geometry, inertia properties and material properties of the slide–crank mechanism are as follows: length of $OA = 0{\cdot}1524$ m (6 in), chord length of $AB = 0{\cdot}3048$ m (12 in), diameter of $AB = 6{\cdot}35 \times 10^{-3}$ m (0·25 in), Young's modulus $E = 2{\cdot}068 \times 10^{11}$ N/m^2 (3×10^7 psi), density $= 7{\cdot}834 \times 10^3$ N s^2/m^4 (7.331×10^{-4} lb s^2/in^4). Three cases are considered for the mass of the sliding block m_s: (a) $m_s = 0$, (b) $m_s = 0.03781$ kg (2.159×10^{-4} lb s^2/in), (c) $m_s = 0.07562$ kg (4.318×10^{-4} lb s^2/in). The initial centroid axis of the coupler is represented by a one-half sine function written as $\bar{v} = \eta \sin(\pi x/l)$, where

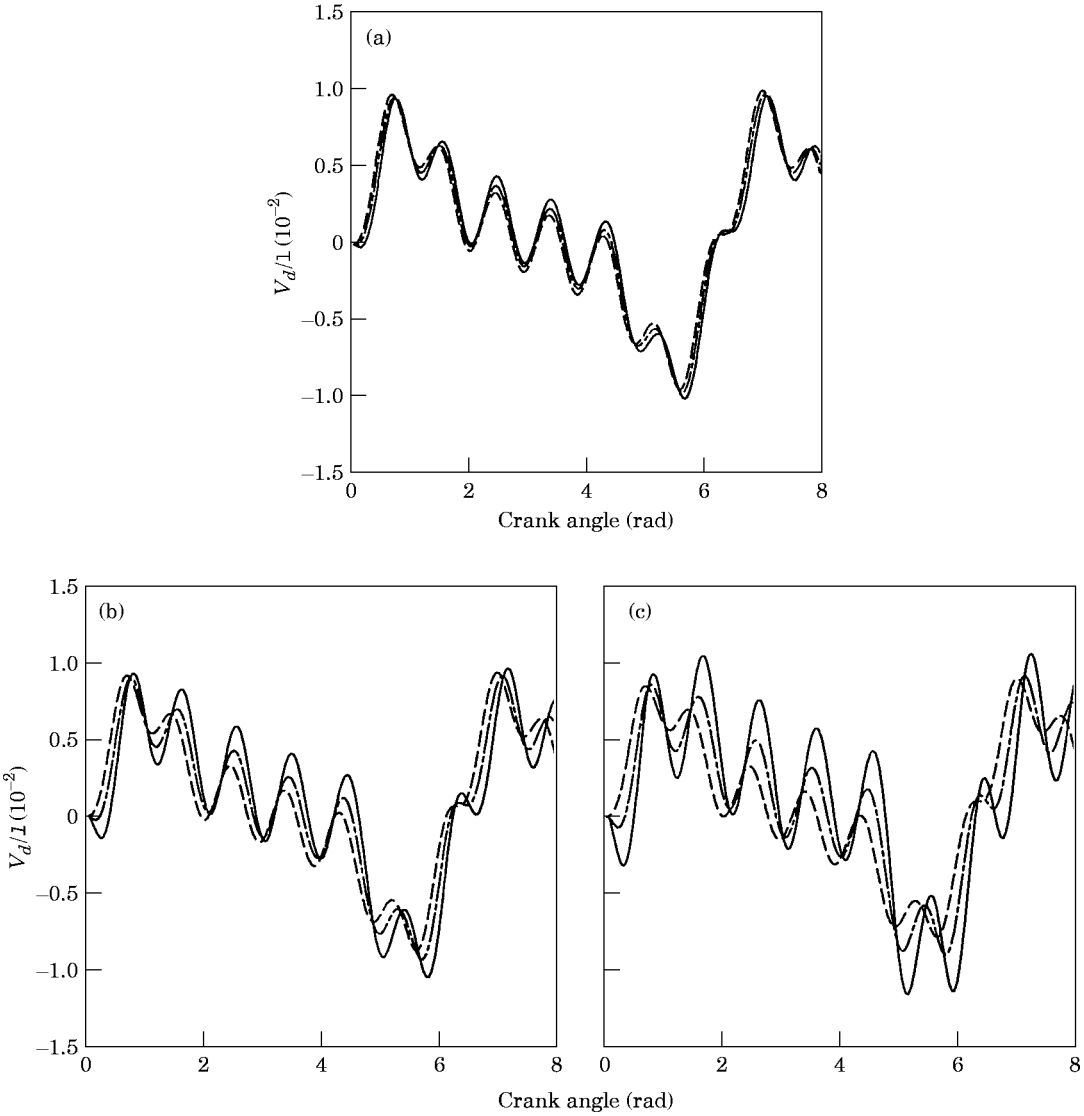

Figure 7. Midpoint deflection of coupler for slider–crank mechanism for $\omega = 124{\cdot}8$ rad/s. (a) $m_s = 0$; (b) $m_s = 0{\cdot}03781$ kg; (c) $m_s = 0{\cdot}07562$ kg. – – –, $\eta/l = 0$; —·—, $\eta/l = 0{\cdot}01$; ——, $\eta/l = 0{\cdot}2$.

η is the amplitude of the sine function and l is the initial chord length of the couple. The values of η/l are chosen to be 0, 0·01 and 0·02 for this example.

The initial crank angle is set to zero and the initial elastic deformations are assumed to be zero. Three different crank speed, $\omega = 124.8$, 250, 375 rad/s are considered here. The initial velocity and acceleration of the mechanism are calculated by using the kinematics of rigid mechanisms. In the numerical study, the rigid crank OA is simulated by a flexible member with the same cross-section and density as the member AB of the Young's modulus 10^{10} times larger than that of member AB. The member OA is discretized by one element for all cases and AB is discretized by using different numbers of element for different cases. Let Δt denote the time step size and N denote the number of elements used for member AB. Unless stated otherwise, Δt is chosen to be 10^{-4}, 5×10^{-5} and

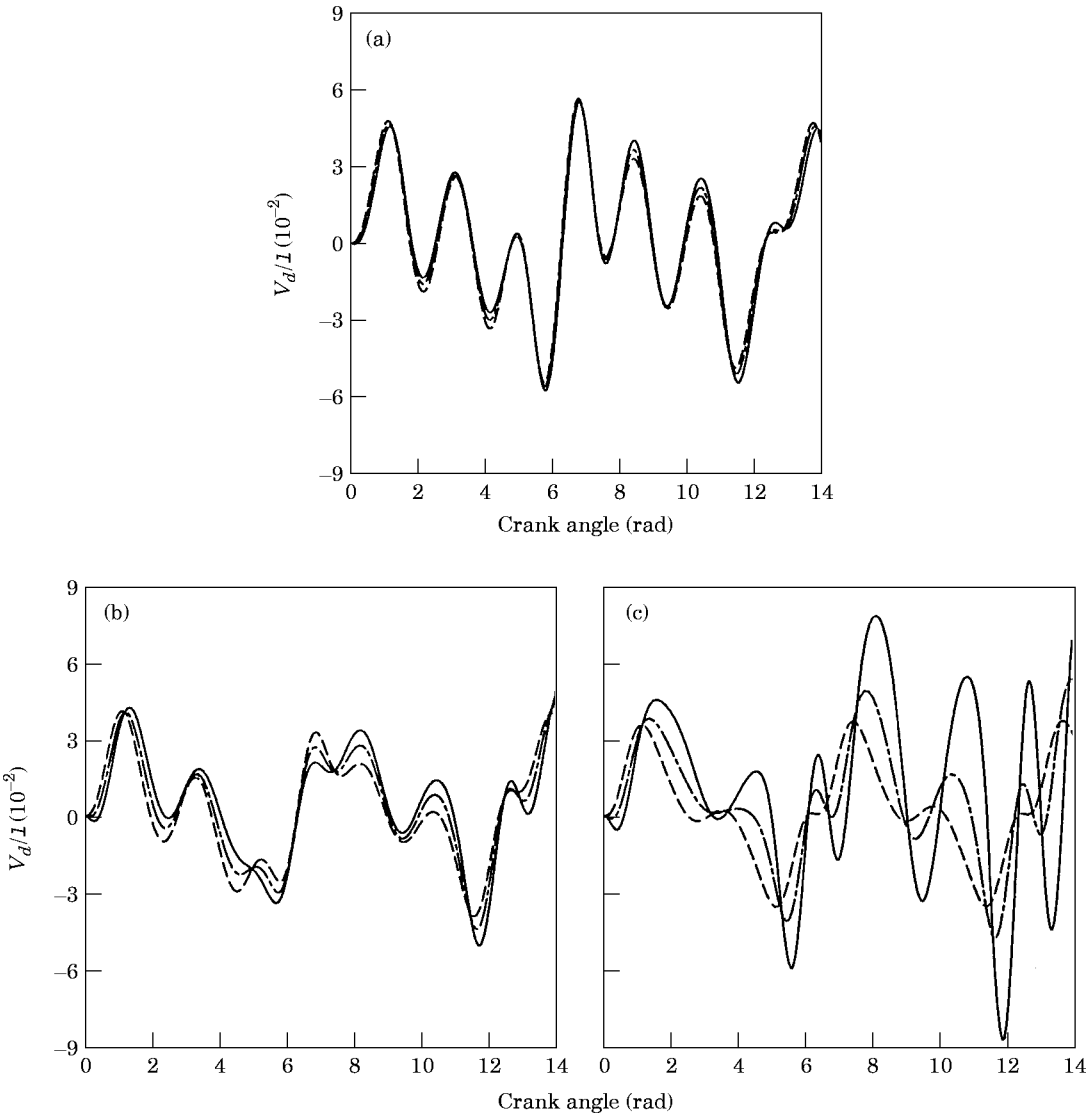

Figure 8. Midpoint deflection of coupler for slider–crack mechanism for $\omega = 250$ rad/s. (a) $m_s = 0$; (b) $m_s = 0{\cdot}03781$ kg; (c) $m_s = 0{\cdot}07562$ kg. – – –, $\eta/l = 0$; —·—, $\eta/l = 0{\cdot}01$; ——, $\eta/l = 0{\cdot}2$.

$2{\cdot}5 \times 10^{-5}$ s, and N is chosen to be 6, 6 and 12 for crack speeds $\omega = 124{\cdot}8$, 250 and 375 rad/s, respectively.

The transverse deflection of the midpoint of the coupler v_d, measured relative to its initial deflection, is computed for different η/l, m_s and ω. For the case $\eta/l = 0$, $m_s = 0$ and $\omega = 124{\cdot}8$ rad/s, the present results obtained when using $N = 2$ are compared with those reported by Chu and Pan [1] in Figure 6. It is seen that the agreement between these two results is very good. Figures 7–9 show the present results for different η/l, m_s and ω. For the cases with $m_s = 0.07562$ kg and $\omega = 375$ rad/s, the results shown in Figure 9(c) were obtained by using $\Delta t = 10^{-5}$ s and $N = 24$. It can be seen that the effect of the initial curvature on the midpoint deflection of the coupler is not negligible for all the cases

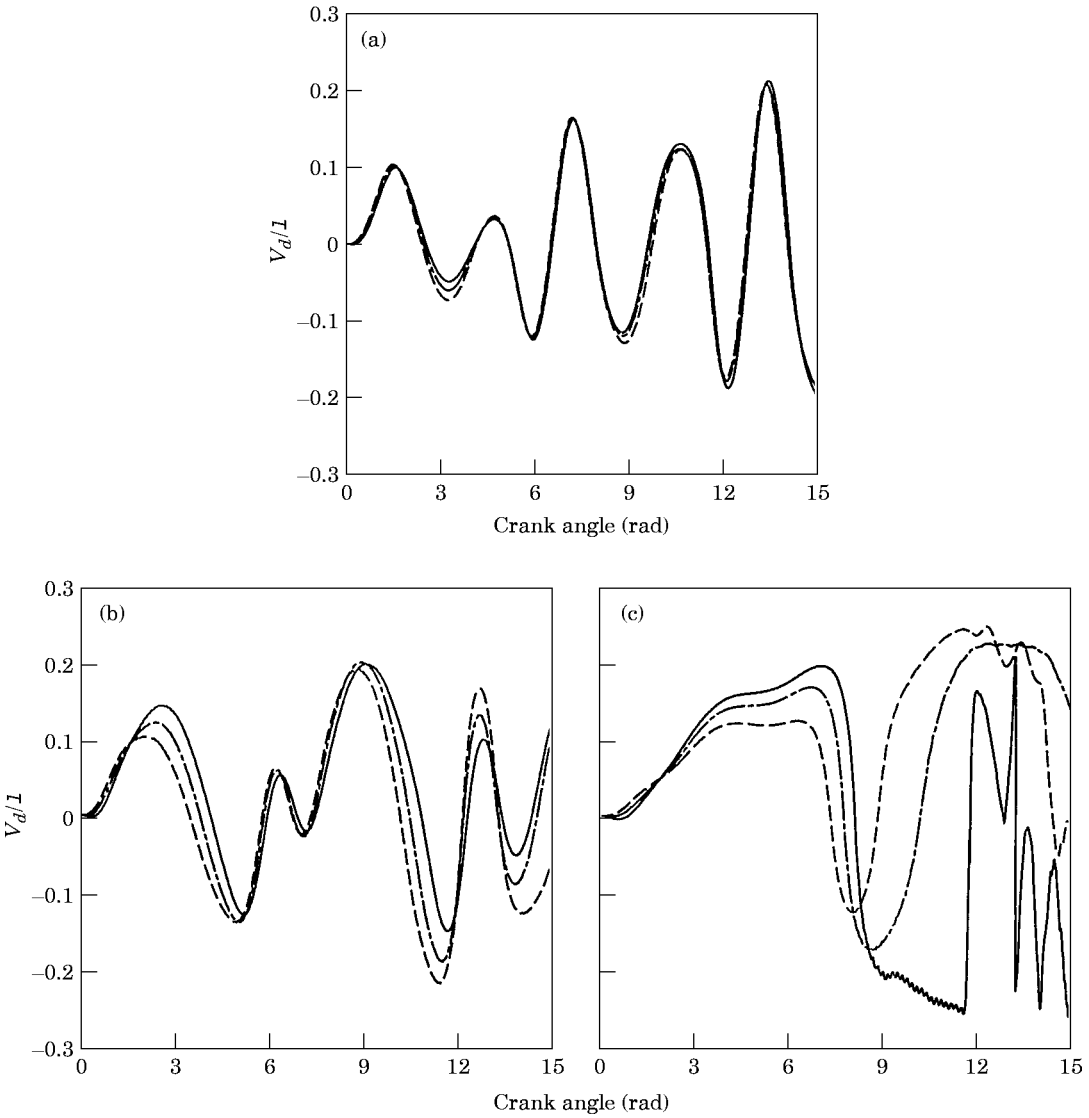

Figure 9. Midpoint deflection of coupler for slider–crank mechanism for $\omega = 375$ rad/s. (a) $m_s = 0$; (b) $m_s = 0{\cdot}03781$ kg; (c) $m_s = 0{\cdot}07562$ kg. – – –, $\eta/l = 0$; —·—, $\eta/l = 0{\cdot}01$; ——, $\eta/l = 0{\cdot}2$.

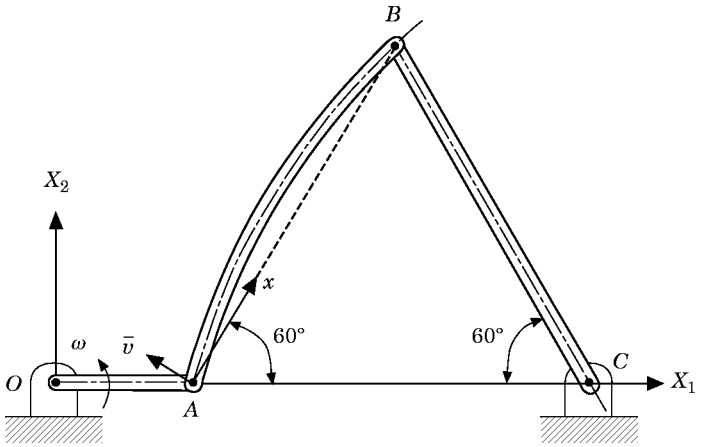

Figure 10. Four-bar mechanism.

studied. The midpoint deflection of the coupler increases with increasing η/l. The discrepancies among the solutions for different η/l increase with increasing m_s and/or ω.

4.2. FOUR-BAR MECHANISM

A four-bar mechanism shown in Figure 10 is considered. The crank OA is considered to be rigid, and the initially curved coupler AB and rocker BC are considered to be flexible. AB and BC are made of the same material and have the same cross section. The geometry, inertia properties and the material properties of the four-bar mechanism are as follows: length of $OA = 0{\cdot}3048\ m$ (12 *in*), chord length of $AB = 0{\cdot}\ 9144$ m (36 in), length of

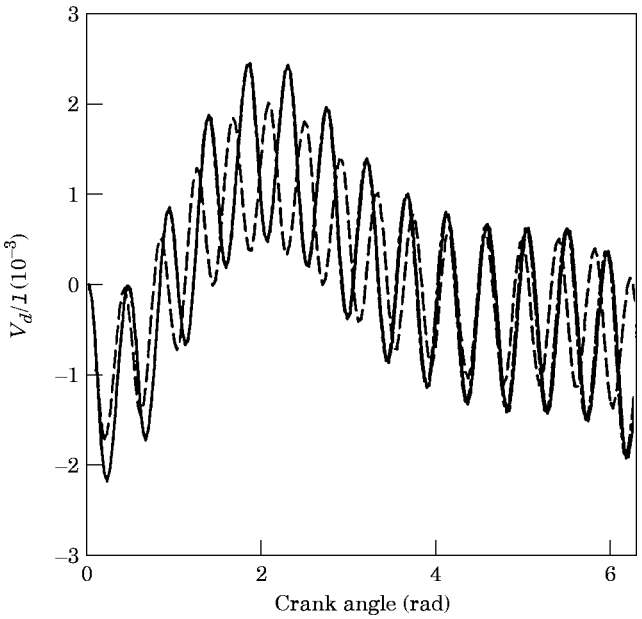

Figure 11. Midpoint deflection of coupler for four-bar mechanism for $\omega = 10\pi$ rad/s. – – –, $\Delta t = 10^{-3}$ s, $N = 1$; — · —, $\Delta t = 10^{-3}$ s, $N = 2$; ——, $\Delta t = 5 \times 10^{-4}$ s, $N = 4$.

$BC = 0{\cdot}9144$ m (36 in) cross section area $= 2{\cdot}58 \times 10^{-3}$ m^2 (4 in^2), moment of inertia $= 1{\cdot}387 \times 10^{-7}$ m^4 ($0{\cdot}3333$ in^4), Young's modulus $E = 7{\cdot}101 \times 10^{10}$ N/m^2 ($1{\cdot}03 \times 10^7$ psi), density $= 2{\cdot}766 \times 10^3$ N s^2/m^4 ($2{\cdot}588 \times 10^{-4}$ lb s^2/in^4). The initial centroid axis of the coupler considered here is the same as those used in the first example.

The initial crank angle is set to zero as shown in Figure 10, and the initial elastic deformations are assumed to be zero. Four different crank speeds, $\omega = 10\pi$, 30π and 60π rad/s are considered here. The initial velocity and acceleration of the mechanism were calculated by using the kinematics of rigid mechanisms. In the numerical study, the rigid crank OA is simulated in the same way as in the first example. The member OA is discretized by one element for all cases, and AB and BC are discretized by the same number of elements. Let N denote the number of elements used for member AB (BC). Unless it is stated otherwise, Δt is chosen to be 5×10^{-4}, $2{\cdot}5 \times 10^{-4}$, $2{\cdot}5 \times 10^{-4}$ and 10^{-4} s, and N is chosen to be 4, 4, 4 and 12 for crank speeds $\omega = 10\pi$, 20π, 30π and 60π rad/s, respectively.

The transverse deflection of the midpoint of the coupler v_d, being measured relative to its initial deflection, was computed for different η/l and ω. For the case $\eta/l = 0$ and $\omega = 10\pi$ rad/s, different Δt and N were used for convergence and accuracy studies. Figure 11 shows the time histories of v_d/l obtained when using $\Delta t = 10^{-3}$ s, $N = 1$,

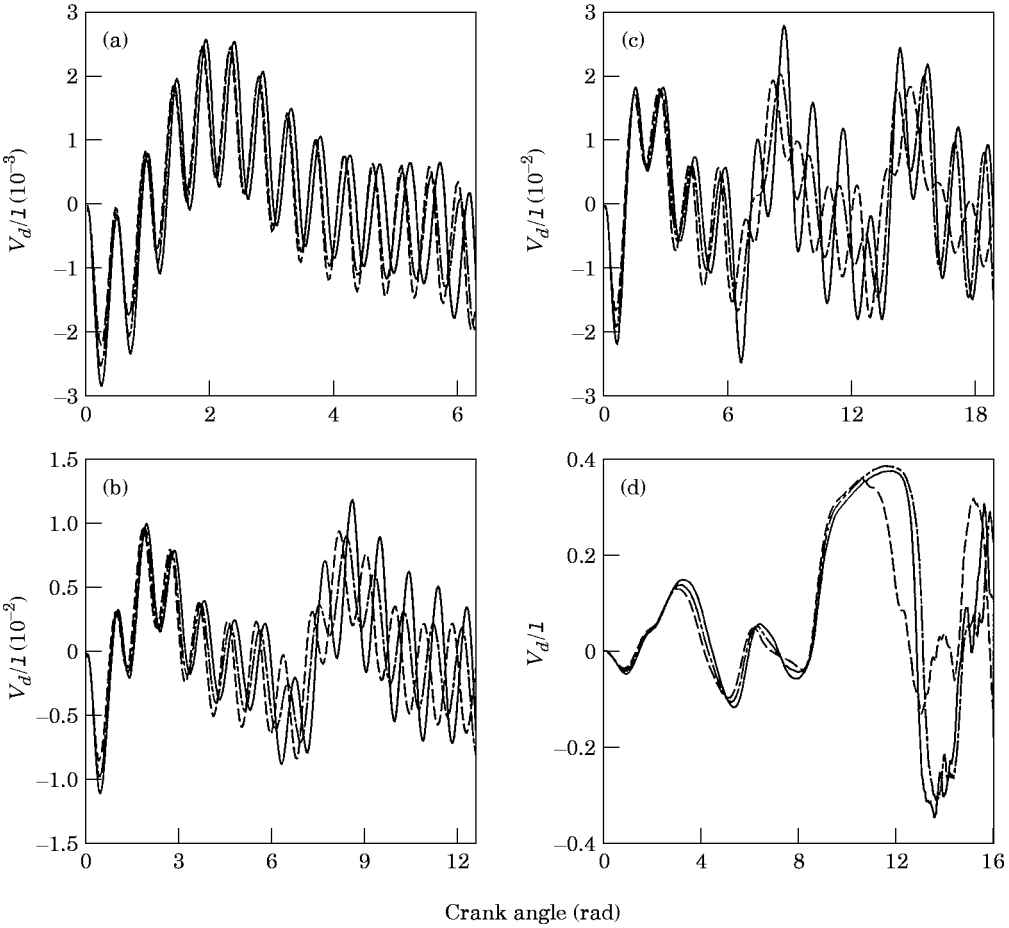

Figure 12. Midpoint deflection of coupler for four-bar mechanism. (a) 10π rad/s; (b) 20π rad/s; (c) 30π rad/s; (d) 60π rad/s. – – –, $\eta/l = 0$; —·—, $\eta/l = 0{\cdot}01$; ——, $\eta/l = 0{\cdot}2$.

$\Delta t = 10^{-3}$ s, $N = 2$, and $\Delta t = 5 \times 10^{-4}$ s, $N = 4$. The solutions corresponding to $\Delta t = 5 \times 10^{-4}$ s, $N = 4$ are nearly identical to those obtained when using $\Delta t = 2 \times 10^{-4}$ s, $N = 4$ (not shown in Figure 11). Thus, the solutions corresponding to $\Delta t = 5 \times 10^{-4}$ s, $N = 4$ may be taken to be the converged solutions. Note that the solutions corresponding to $\Delta t = 10^{-3}$, $N = 1$ are nearly identical to those reported in reference [9] (not shown in Figure 11), which were obtained by using the same Δt and N. As can be seen from Figure 11, the solutions obtained by using $\Delta t = 10^{-3}$, $N = 1$ are not accurate enough. Figure 12 shows the present results for different η/l and ω. It can be seen that the effect of the initial curvature on the midpoint deflection of the coupler is not negligible for all the cases studied. The midpoint deflection of the coupler increases with increasing η/l. The discrepancies among the solutions for different η/l increase with increasing ω.

5. CONCLUSIONS

A co-rotational finite element formulation of a slender curved beam element to investigate the effect of member initial curvature on the dynamic behaviour of planar flexible mechanisms has been presented. The Euler–Bernoulli hypothesis and the initial curvature are properly considered for the kinematics of curved beams. Both the inertia nodal forces and deformation nodal forces are systematically derived by consistent linearization of the fully geometrically non-linear beam theory by using the d'Alembert principle and the virtual work principle. In conjunction with the co-rotational formulation, the higher order terms of the nodal parameters in the element nodal forces are consistently neglected. From the numerical examples studied, it is found that the effects of the initial curvature on the dynamic response of flexible mechanisms is not negligible for all the cases studied. The midpoint deflection of the coupler increases with increasing η/l. The discrepancies among the solutions for different η/l increase with increasing ω.

It is believed that the consistent co-rotational formulation for a curved beam element presented here may represent a valuable engineering tool for the dynamic analysis of planar flexible mechanisms with initially curved members.

ACKNOWLEDGMENTS

The research was sponsored by the National Science Council, Republic of China, under the contract NSC79-0401-E009-15.

REFERENCES

1. S. C. Chu and K. C. Pan 1975 *ASME Journal of Engineering for Industry* **97,** 542–550. Dynamic response of a high-speed slider–crank mechanism with an elastic connecting rod.
2. J. O. Song and E. J. Haug 1980 *Computer Methods in Applied Mechanics and Engineering* **24,** 359–381. Dynamic analysis of planar flexible mechanisms.
3. A. K. Noor and N. F. Knight 1980 *Computer Methods in Applied Mechanics and Engineering* **23,** 225–251. Nonlinear dynamic analysis of curved beams.
4. M. Badlani and A. Midha 1982 *ASME Journal of Mechanical Design* **104,** 159–167. Member initial curvature effects on the elastic slider–crank mechanism response.
5. J. C. Simo and Vu-Quoc 1987 *Journal of Sound and Vibration* **119,** 487–508. The role of non-linear theories in transient dynamic analysis of flexible structures.
6. T. R. Kane, R. R. Ryan and A. K. Banerjee 1987 *Journal of Guidance, Control and Dynamics* **10,** 139–151. Dynamics of a cantilever beam attached to a moving base.
7. D. F. Bartolone and A. A. Shabana 1989 *Mechanism and Machine Theory* **24,** 411–429. Effect of beam initial curvature on the dynamics of deformable multibody systems.

8. S. K. IDER and F. M. L. AMIROUCHE 1989 *ASME Journal of Applied Mechanics* **56,** 444–450. Nonlinear modeling of flexible multibody systems dynamics subjected to variable constraints.
9. F. W. LIOU and A. G. ERDMAN 1989 *ASME Journal of Vibrations*, *Acoustics*, *Stress*, *and Reliability* **111,** 35–47. Analysis of high-speed flexible four-bar linkage, part I: formulation and solution. Part II: analytical and experimental results of the Applo.
10. K. M. HSIAO and J. Y. JANG 1989 *Computers and Structures* **33,** 1057–1063. Nonlinear dynamic analysis of elastic frames.
11. Z. YANG and J. P. SADLER 1990 *ASME Journal of Mechanical Design* **112,** 175–182. Large-displacement finite element analysis of flexible linkages.
12. K. M. HSIAO and J. Y. JANG 1991 *Computer Methods in Applied Mechanics and Engineering* **87,** 1–14. Dynamic analysis of planar flexible mechanisms by co-rotational formulation.
13. K. M. HSIAO, R. T. YANG and A. C. LEE 1994 *International Journal for Numerical Methods in Engineering* **37,** 75–89. A consistent finite element formulation for nonlinear dynamic analysis of planar beam.
14. T. J. CHUNG 1988 *Continuum Mechanics*. Englewood Cliffs, NJ: Prentice Hall.
15. D. H. HODGES 1988 *AIAA Journal* **22,** 1825–1827. Proper definition of curvature in nonlinear beam kinematics.
16. K. J. BATHE 1992 *Finite Element Procedures in Engineering Analysis*. Englewood Cliffs, NJ: Prentice Hall.